A Temperature Sensor with A Water-Dissolvable Ionic Gel for Ionic Skin

Shunsuke Yamada[1,2]*, *Hiroshi Toshiyoshi*[2]

[1]Research Organization for Nano & Life Innovation, Waseda University, 3-4-1 Ookubo, Shinjuku, Tokyo 169-8555, Japan

[2]Institute of Industrial Science (IIS), The University of Tokyo, 4-6-1 Komaba, Meguro-ku, Tokyo 153-8505, Japan.

KEYWORDS: Temperature sensor, Ionic liquid, Polyvinyl alcohol, Electrical double layer, Water dissolvable

ABSTRACT

In the era of trillion sensors, a tremendous number of sensors will be consumed to collect information for big data analysis. Once they are installed in harsh environment or implanted in a human/animal body, we cannot easily retrieve the sensors; the sensors for these applications are left unattended but expected to decay after use. In this paper, A disposable temperature sensor that disappears by contact with water is reported. The gel electrolyte based on an ionic liquid and a water-soluble polymer, so called ionic gel, exhibits the Young's modulus of 96 kPa, which is compatible with human muscle, skin, and organs, as wearable devices or soft robotics. A study on

electrical characteristics of the sensor with various temperature reveals that the ionic conductivity and capacitance increased by 12 times and 4.8 times, respectively, when the temperature varies from 30˚C to 80˚C. The temperature sensor exhibits a short response time of 1.4 s, allowing real-time monitoring of temperature change. Furthermore, sensors in an array format can obtain the spatial distribution of temperature. The developed sensor was found to fully dissolves in water in 16 hours. The water-dissolvability enable practical applications including healthcare, artificial intelligence, and environmental sensing.

1. Introduction

In the era of trillion sensors, a tremendous number of sensors will be consumed to collect information for big data analysis, including tactile[1–5], temperature[6–10], and biomimetic sensors[11–13]. Once they are installed in harsh environment or implanted in a human/animal body, we cannot easily retrieve the sensors; the sensors for the above applications are required to be left unattended but disappear after use. One of the advantages of such a sensor is reduction of waste and cost. The self-disappearance is essential as well in terms of the elimination of the sensor retrieval from human body to reduce the physical damage by the surgery. The biodegradable devices have been proposed by using organic and inorganic hybrid devices to obtain high functionality[14–18]; for instance, G. A. Salvatore et al. reported a temperature sensor based on biodegradable materials[14]. Such a sensor should disappear immediately after prescribed time for data acquisition[14,15]. Water is abundant in human body and environment, and can works as a trigger to decompose materials. One of the potential applications is agriculture. Environmental monitoring enables us to control growth of vegetables and predict the time to harvest. Biodegradable temperature sensor embedded into the soil could eliminate the sensor retrieval because of self-dissolution. S. W. Hwang et al.

utilized silicon, silicon dioxide, and magnesium to develop a biodegradable and bioresorbable implantable sensing system[15], which gradually decomposed after contact with water. A chemical sensor and biosensor are crucial to detect chemical substances in a human body. Temperature sensor is also essential to calibrate the response of the sensors because the chemical sensors and biosensors shows temperature dependency[19]. Nevertheless, the conventional biodegradable temperature sensors show the small change of the resistance in respect to temperature owing to the small temperature coefficient for resistivity. Furthermore, a lack of the mechanical flexibility prevents the temperature sensors from applications to flexible and stretchable electronics.

Recently, researchers employed ions as a carrier for flexible devices, so-called ionic skin (i-skin)[20]. Typical i-skin consists of a hydrogel, and exhibits large mechanical deformation under physical stimulus. Furthermore, most hydrogels are biocompatible in human body, thereby enabling us to develop an implantable device for health monitoring. The conventional i-skin adopted hydrogel, and was subject to the evaporation of moisture. The loss of solvent changes the ionic conductance, which make it difficult to use the device in dry conditions.

Ionic liquids (ILs) have been, recently, adapted to enhance the electrical characteristics of organic devices[21–25]. The IL consists of two types of molecules with positive and negative charges, and it shows unique characteristics. The IL, for instance, is a non-volatile liquid at room temperature and pressure due to the large molecular weights of the cations and anions which hinder the crystallization of the IL. The IL forms quite a thin layer on the electrode, upon application of voltage, which exhibits an extremely large electrical capacitance of several μF/cm^2. The IL shows high ionic conductivity as well, and these values remain high even when the IL is suspended in an ionic gel (IG) that uses polymer networks including poly(vinyl alcohol) (PVA)[26,27], poly(ethylene oxide) (PEO)[28,29], and poly(ethylene glycol) (PEG)[30]. As temperature increases, the viscosity of the

ionic liquid reduces[31–33], which increases ionic conductivity by increasing ion mobility. The dissociation of the ions is activated in high temperature; the ionic conductivity and the capacitance of the IL are enhanced with temperature due to the increase of the charge carrier[34,35]. Certain ILs possess biodegradability and non-toxicity, which enables us to develop IL-based eco-friendly devices for disposable use.

In this paper, we report on a biodegradable temperature sensor to monitor the temperature in the range between 30˚C and 80˚C by using IL, tris(2-hydroxy-ethyl) methylammonium ethylsulfate ($[MTEOA]^+[MeOSO3]^-$), and PVA. The IL and PVA materials exhibit biodegradability and environmentally safety[36–39], and so does the proposed IG.

The conductivity and capacitance of the IG increased by 12 and 4.8 times, respectively, with the temperature increase from 30˚C to 80˚C. We confirmed the optical transparency of the IG in the visible wavelength range; these properties are promising for the integration with light emitting devices. The developed IG shows a Young's modulus of 96 kPa, which is as compliant as human body including blood vessel, skin, and muscle[40–42] for biomechanical compatibility when used as an implanted device. The temperature sensor was found to disappear 16 hours after soaking into deionized water (DIW) due to the water-dissolvable nature of PVA.

2. Results and Discussion

2.1 Device fabrication.

Figure 1a illustrates a schematic design of the arrays of the temperature sensors which consist of the metal-IG-metal configuration as shown in **Figure 1b**. The temperature sensor was developed by using a shadow mask and transfer printing as shown in **Figure 1c**. A PVA film was formed on a glass substrate (Matsunami, S9213) by using a bar coater. The thickness of the PVA film was of

60 μm as described in Supporting Information (see Figure S1). The electrodes of the cupper foil were patterned by using a laser processing machine (LPKF Laser & Electronics KK, ProtoLaser U3), and transferred on to the PVA sheet as lower electrodes. The IG precursor was casted into a polyimide shadow mask for patterning, and dried to form the gel. The transfer of the upper electrodes on the IG yielded temperature sensor arrays. The device was annealed at 100 ˚C for 1 hour in the glovebox filled with nitrogen to remove the residual moisture in the device. **Figure 1d** shows photograph of the temperature sensor arrays. The magnified view of the unit cell shown in **Figure 1e** indicates that the upper and the lower electrodes were aligned well. The mechanical flexibility of the materials exhibited an ability to bend in a small radius of curvature as shown in **Figure 1f**.

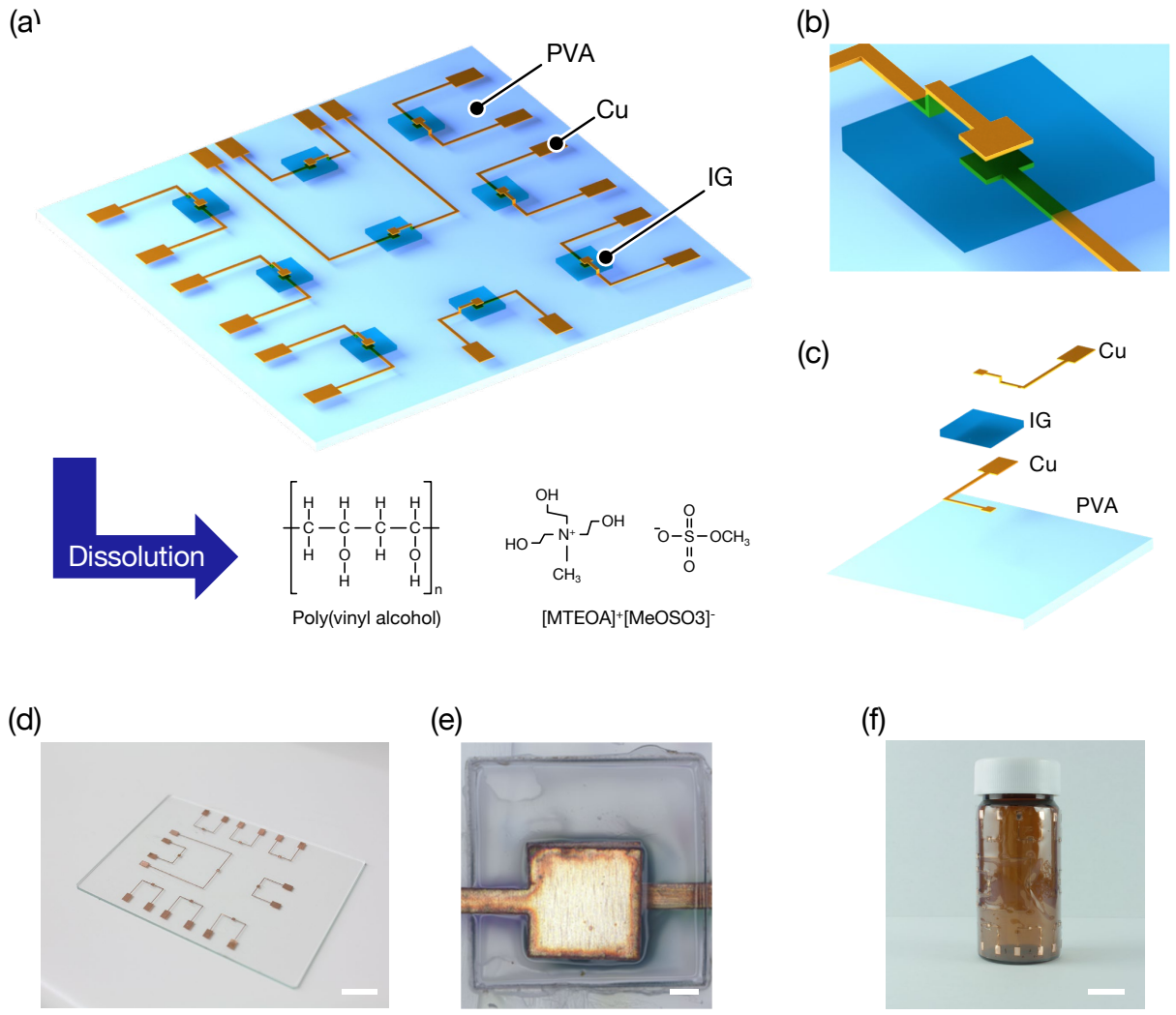

Figure 1. Schematic illustrations and photographs of the temperature sensor. (a) Illustration of an array of the temperature sensor which is composed of a PVA and an ionic gel. The sensor dissolves by a contact with water. (b) Design of the temperature sensor using copper foil. (c) Schematic illustration for the fabrication process of the sensor. The ionic gel precursor was coated on the electrode using the stencil mask followed by the transfer of the lower electrodes on the PVA sheet. The transfer of the upper electrodes forms the metal-ionic gel-metal configuration. (d) Photograph of the 3 × 3 sensor array and (e) magnified view of the unit cell (scale bar, 10 mm). (f) The sensor exhibits flexibility (scale bar, 10 mm).

2.2 Mechanical and optical characteristics.

The compatibility to the human skin is required for the wearable devices to monitor the vital signs without discomfort. The IG exhibited flexibility as shown in **Figures 2a** and **b**. To investigate the mechanical property, we carried out a tensile stress test of the IG and PVA. **Figure 2c** shows the photograph of the experimental bed with a tensile tester (ZwickRoell, Z0.5). The layout for the samples is described in Supporting Information (see Figure S2). The PVA shows the tensile curves of polymeric substances as shown in **Figure 2d**; the stress increased linearly in the elastic region, followed by the nonlinear region after the strain exceeded the elastic limit. The IG exhibited lower stress than that of the PVA in the same strain range. The IG fracture strain was of 169%, which value was larger than that of the PVA with the fracture strain of 140%. The Young's moduli of the PVA and IG obtained by the least square method in the linear region of the stress-strain curves were of 1.4 MPa and 97 kPa, respectively. The IG becomes softer than the PVA because it was composed of the liquid of more than 50% weight, thereby allowing the liquid to move through the polymer matrix to deform as the stress is provided. Those Young's moduli are equivalent to those of human body, for example, skin (420 kPa ~ 850 kPa)[43], the a blood vessel (430 kPa ~ 870 kPa)[44], and muscle (medial gastrocnemius muscle:15 kPa ~ 30 kPa, lateral gastrocnemius muscle:15 kPa~30 kPa , Achilles tendon: 250 kPa ~ 500 kPa)[45] . Previous works using metal or inorganic semiconductor achieved flexible electronic devices by reducing the thickness to as small as a few tens of nm[10,46,47]. Such devices need vacuum processes and photolithography steps, which fail to achieve large-scale and low-cost fabrication. On the other hand, gels are intrinsically soft, and hence they do not have to be in a thin thickness for mechanical flexibility; this feature allows large-scale and low-cost fabrication of flexible devices, e.g. screen printing.

The transparent materials are intriguing to develop a flexible application which requires visibility of the supporting substrate such as a touch panel on a display[20], optogenetics[48], and actuator[49]. One of the applications of the actuator is a haptic device combined with a display to provide an image with texture. The haptic device emulates the texture by the vibration, and should be transparent to be installed on the surface of the display to transmit it without loss. The PVA can be employed as a light polarizer[50]. The polarizer is composed of the PVA film and an iodide compound. The transparency of the PVA is essential for the transmission of the light without optical attenuation. Furthermore, extensibility of PVA is also essential because the optical polarization behavior is developed by mechanically stretching the polymer and iodide compound coating. The high transparency of the PVA to visible and IR light enables us to develop transparent soft electronics using the transparent ionic liquid. The developed IG exhibited the transparency such that the red, green, and blue pixels were clearly visible through the IG sheet as shown in **Figure 2(e)**. To quantitatively investigate the transparency, **Figure 2(f)** shows the optical transmittance of the IG using a UV/Vis spectrophotometer (JASCO Germany, V-630) in the range of wavelength from IR to UV. The transmittance of the 100 μm thick IG and PVA films remained as high as 90% in the broad spectrum from IR to visible light. The IG transparency is comparable with that of a 1-mm thick glass plate as depicted with black dash line in **Figure 2(f)**, which enables us to integrated the ionic devices of the IGs with the display or LED devices.

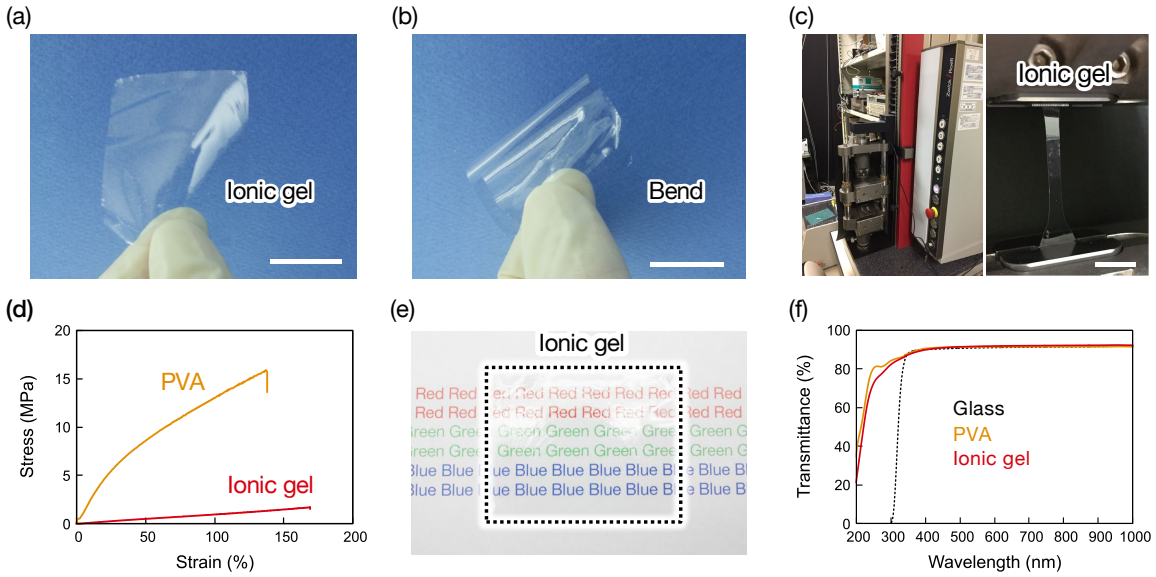

Figure 2. Mechanical and optical characteristics of the ionic gel. (a) Schematic image and (b)photographs of the ionic gel (scale bar, 10 mm). (c) Experimental bed for the tensile stress test (scale bar, 10 mm). (d) Tensile curves of the PVA and ionic gel. (e) Ionic gel is transparent to red, blue, and green colors. (f) Transmittance of the ionic gel in the various wavelength of the light.

2.3 Temperature sensor characteristics.

The temperature sensor was developed based on the electrical characteristics of the ionic liquid due to the temperature-dependent dissociation of the ions[34,51] as schematically shown in **Figure 3a**. The electrical characteristics were investigated by measuring the impedance $\boldsymbol{Z}$, phase angle $\boldsymbol{\theta}$, and capacitance $\boldsymbol{C}$ of the IG in the temperature range between 30˚C and 80˚C with the experimental bed as shown in **Figure 3b**. **Figure 3c** shows the change of absolute values of the impedance $|\boldsymbol{Z}|$ and phase angle. The $|\boldsymbol{Z}|$ reduced as temperature increased due to the dissociation of the ions. The increase of the charge carrier resulted in the enhancement of the ionic conductivity and decrease of the $|\boldsymbol{Z}|$ over one order of magnitude at the frequency of 100 kHz. **Figure 3d** shows the change

of the ***C*** at various temperatures. The increase of ***C*** at 1 Hz is explained by the decoupled charges at the interface between the IG and electrode as well. The coupled ions hinder the accumulation of the ions at the interface to decrease the charges associated with electrical double layer capacitance. At an elevated temperature, the decoupled ions accumulated at the interface to form the electrical double layer, and thereby increasing capacitance of the IG. These electrical shifts are obvious in the phase shift as shown in **Figure 3c**. In the low frequency regime, the IG shows a reduction in phase by several tens of degrees, being associated with enhancement of the electrical double layer capacitance. The increase of the ionic conductivity allows for the capacitive response against the electrical signals of the high frequency, which results in the drop of the phase in the high frequency range.

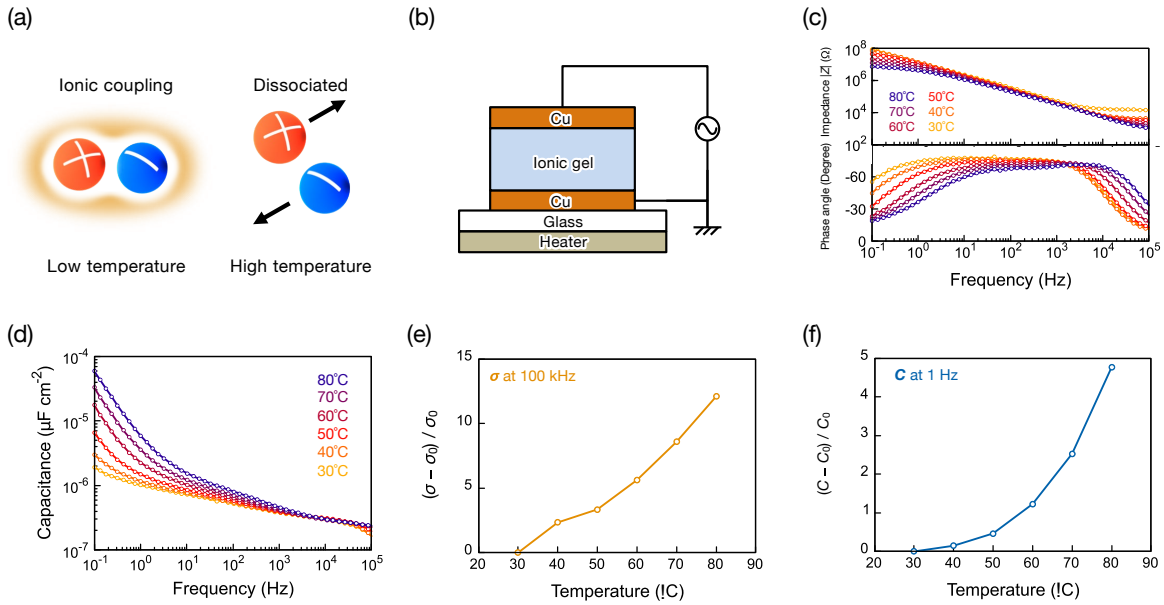

Figure 3. Fundamental temperature response of the sensor. (a) Mechanism of the temperature sensing with ionic liquid. (b) Experimental setup for the measurement with a sensor unit cell. (c) Bode diagram and (d) the capacitance of the sensor with the temperatures between 30˚C and 80˚C. Changes of (e) conductivities and (f) capacitance with increasing and desecreasing temperature.

Figures 3e and **3f** respectively show the ionic conductivity and capacitance response to the temperature change from 30˚C to 80˚C. Those of responsivities are defined by $(\boldsymbol{\sigma} - \boldsymbol{\sigma}_0)/\boldsymbol{\sigma}_0 = \Delta\boldsymbol{\sigma}/\boldsymbol{\sigma}_0$ and $(\boldsymbol{C} - \boldsymbol{C}_0)/\boldsymbol{C}_0 = \Delta\boldsymbol{C}/\boldsymbol{C}_0$, where $\boldsymbol{\sigma}_0$ and $\boldsymbol{C}_0$ are the conductivity and capacitance at the frequency of 100 kHz and 1 Hz, measured at 30˚C, respectively. The ratios $\Delta\boldsymbol{\sigma}/\boldsymbol{\sigma}_0$ and $\Delta\boldsymbol{C}/\boldsymbol{C}_0$ were found to increase by 12 and 4.8 times as the temperature elevated from 30˚C to 80˚C, respectively. The previous studies reported that those values increased linearly with temperature[34]. On the other hand, the change of the capacitance increased nonlinearly in this work. In an ionic liquid, coulomb forces, hydrogen bonds and van der Waals forces are present[52–54]. While the ionic liquid in the previous study[34] is relatively hydrophobic due to the hydrophilic–hydrophobic properties of ions[55], the hydrogen bonds in $[MTEOA]^+[MeOSO3]^-$ may enhance the activation energy to dissociate those bondings by temperature increase, and have resulted in the nonlinear electrical performance.

2.4 Measurement of noise level.

Low noise level of the sensor over time is essential for precise temperature monitoring. For testing, the developed sensor was held on the hotplate at a constant temperature of 30˚C to monitor the noises of $\boldsymbol{\sigma}$ and $\boldsymbol{C}$. **Figures 4a** and **4b** display the impedance and capacitance noise for 300 seconds, defined as $(\boldsymbol{\sigma} - \boldsymbol{\sigma}_{ave})/\boldsymbol{\sigma}_{ave}$ (%) and $(\boldsymbol{C} - \boldsymbol{C}_{ave})/\boldsymbol{C}_{ave}$ (%), where $\boldsymbol{\sigma}_{ave}$ and $\boldsymbol{C}_{ave}$ are respectively the averages of the conductivity at 100 kHz and capacitance at 1 Hz. The noise of $\boldsymbol{\sigma}$ and $\boldsymbol{C}$ were up to 1.4% and 0.5%, respectively, which are sufficiently small for the measurement of the temperature.

2.5 Response time to temperature change.

We then characterized the response time of the temperature sensor. The conductivity and the capacitance of the temperature sensor were monitored by placing a glass plate of 60˚C on the

sensor. **Figures 4d** and **4e** show the change of the conductivity and capacitance of the temperature sensor, respectively. The sensor remained at 25˚C before the glass plate transfer; the values of $\Delta\boldsymbol{\sigma}/\boldsymbol{\sigma}_0$ and $\Delta\boldsymbol{C}/\boldsymbol{C}_0$ were both negative. When the glass plate was transferred on the sensor, the $\Delta\boldsymbol{\sigma}/\boldsymbol{\sigma}_0$ and capacitance $\Delta\boldsymbol{C}/\boldsymbol{C}_0$ increased to 0.3 and 0.23 in 1.4 s and 4 s, respectively. Note that the interval time for the measurement of the $\boldsymbol{\sigma}$ was of 0.05 s with the input signal frequency of 100 kHz. On the other hand, the capacitance was measured every 2 s, as the frequency used for the capacitance measurement was as low as 1 Hz; the response time of such measurement is 4 s.

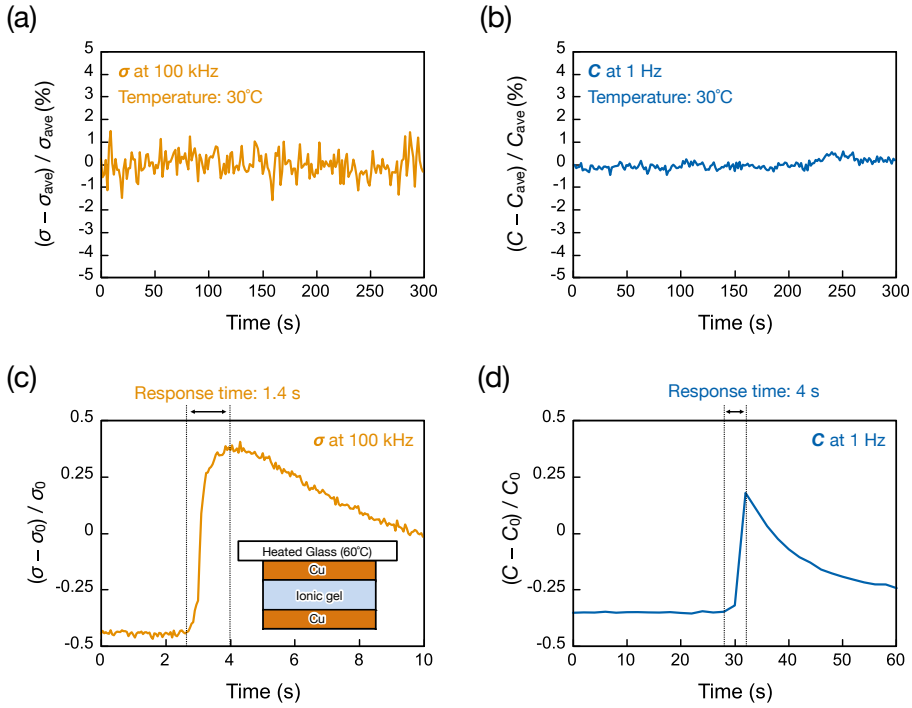

Figure 4. Ionic gel performance of electrical characteristics over time. Noise level of the (a) ionic conductivity and (b) capacitance at 100 kHz and 1 Hz, respectively. Upon transfer of the hot glass plate, the (c) ionic conductivity and (d) capacitance vary within 1.4 s and 4 s, respectively.

2.6 Multipoint temperature sensing.

The i-skin has benefits to measure vital signs of humans in the large area at a high resolution. Forming arrays to monitor distribution of the temperature is advantageous for the applications of the healthcare. The proof-of-concept matrix-type temperature sensor was developed with nine temperature sensors arranged in a 3 × 3 format with the size of 5 cm × 5 cm as shown in **Figure 5a**, where a conductive tape was used to ensure electrical contacts. Although the IG is optical transparent as shown in **Figure 2e** and **2f**, considerable part of the device is opaque owing to the metallic copper electrodes. According to the previous research on transparent electrodes, a fully transparent temperature sensor is possible by using a transparent conductive polymer[57], an extremely thin metal electrode[58], or a metal electrode with grid structures[48]. **Figure 5b** shows the photograph of the experiment to investigate the sensor response to the placement of an electronic hand warmer with the temperature of 55˚C, where the $\boldsymbol{\sigma}$ was monitored. **Figures 5c** and **5d** show the $\Delta\boldsymbol{\sigma}/\boldsymbol{\sigma}_0$ of the temperature sensor with and without the electronic hand warmer at the temperature of 30˚C, respectively, where the bars represent the $\Delta\boldsymbol{\sigma}/\boldsymbol{\sigma}_0$ at each pixel. The points with high conductivity (or high temperature) corresponded well with the position of the electronic hand warmer. For now, the size of the sensing area was as large as 1 mm^2, which could be made smaller by using the microelectromechanical system (MEMS) technology.

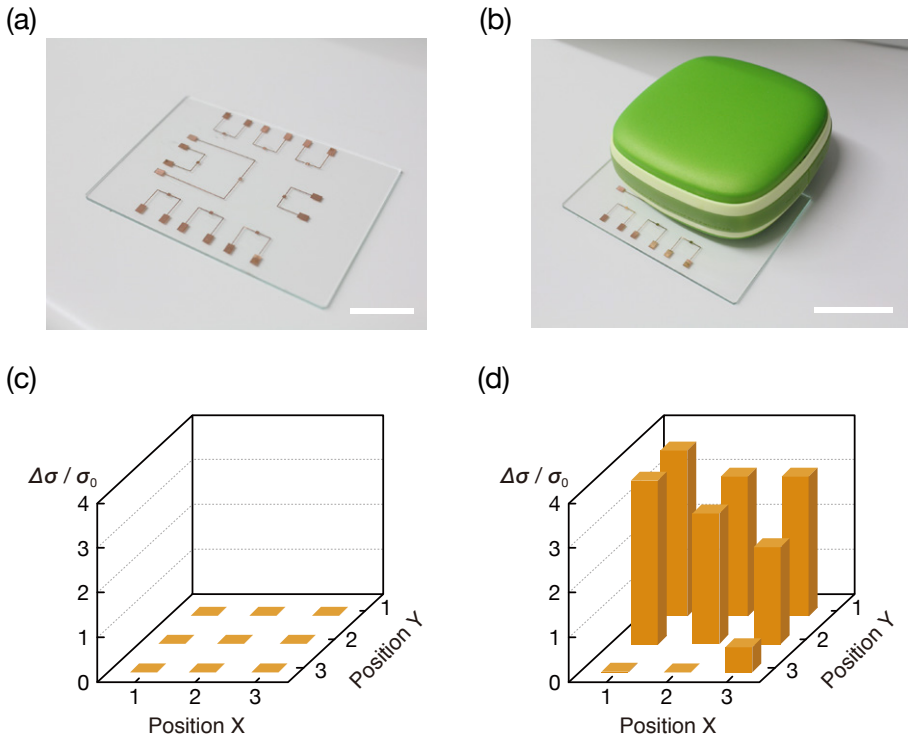

Figure 5. Array of temperature sensor for multipoint sensing. Photographs of sensor matrix (a) without (scale bar, 20 mm) and (b) with a hand warmer (scale bar, 30 mm). The response of the $\Delta\sigma/\sigma_0$ (c) before and (d) after the placement of the hand warmer.

2.7 Device dissolution into water.

The change of the electrical behavior was monitored while soaking the sensor into the DIW, which was warmed to 60˚C to accelerate the dissolution. **Figures 6a and 6b** show the photograph of the sensor on the glass substrate before and 40 minutes after dipping in DIW. The electrodes peeled off from the PVA film and IG due to the dissolution of the substrate. The ionic gel and PVA film were fully dissolved in 16 hours. Note that the copper did not dissolve into DIW because it was as thick as 10 μm. The previous research reports that thin films of molybdenum (300 nm) dissolves

into the DIW in 9 days[59]. We will substitute the electrode with water-soluble metal such as molybdenum to develop completely water-soluble temperature sensor.

Figure 6c shows the change of the impedance and phase angle. The dissolution of the IG resulted in the loss of ions, and reduction of the ionic conductivity at high frequency of 100 kHz. The change of the ionic conductivity was also verified by the shift of phase from −11˚ to −76˚ at 100 kHz; the electrical performance of the metal-IG-metal configuration changed from conductive nature to capacitive. The dissolution of the IG also had the influence on capacitance of the IG. The reduction of the capacitance in the high frequency regime was verified as large as one order of magnitude due to the loss of the IL.

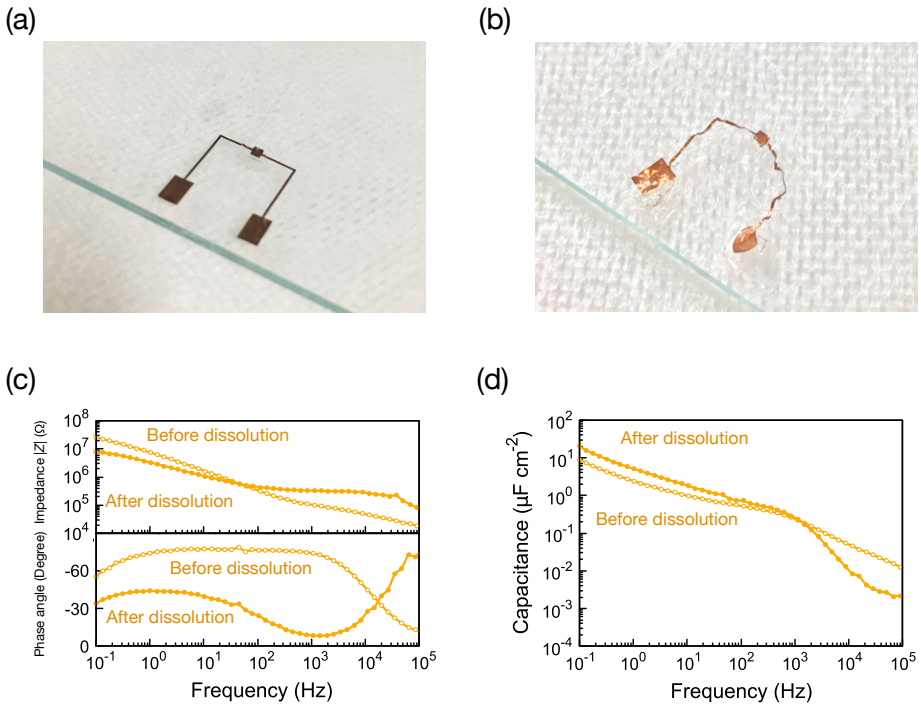

Figure 6. Dissolution into deionized water. The photograph of the sensor (a) before and (b) after dissolution. The electrical characteristics of: (c) impedance and phase angle, and (d) capacitance before and 40 minutes after dissolution of the sensor.

3. Conclusion

A water dissolvable temperature sensor has been developed by using ionic gel and PVA. A study on the electrical characteristics in regards to the temperature reveals that temperature shift from 30˚C to 80˚C has an effect to increase the ionic conductance and capacitance change by 12 and 4.8, respectively. The short response time of 1.4 s enables to monitor the real-time change of temperature. Moreover, the array of the temperature sensor with the 3 × 3 configuration allows to monitor the spatial distribution of temperature. The sensor was found to fully dissolve into DIW in 16 hours. This work shows a disposable sensor based on the ionic liquid of biodegradability and water-dissolvability, which could be deployed in practical applications including healthcare, and environmental sensing.

4. Experimental Section

Preparation of ionic gel precursor: We used commercially available ionic liquid (IL), $[MTEOA]^+[MeOSO_3]^-$ (Sigma-Aldrich, catalog ID: 91198) and PVA powder (Sigma-Aldrich, molecular weight 89,000-98,000, 99+% hydrolyzed, catalog ID:341584) without further purification. We dissolved the PVA into DIW at 90 ˚C to liquefy, where weight ratio of the PVA and DIW is 1:8. The solvent was thoroughly stirred at the 900 rpm for 30 minutes, and IL was added and homogenized to make the ionic gel precursors at the IL weight ratio of 60 wt% with respect to the PVA. The solvent contained the PVA, DIW, and IL with the weight ratio of 2:16:3.

Device fabrication: As of temperature sensor, the PVA solvent was casted on a glass substrate, and coated by using a bar coater to obtain a uniform PVA sheet. The glass was kept in the ambient

air for 1 day to evaporate the DIW. The 4 μm thick copper foil was patterned by using a laser processing machine (LPKF Laser & Electronics KK, ProtoLaser U3), and transferred on the PVA sheet as a lower electrode. To pattern the IG, the polyimide sheet cut by a laser processing machine was used as a shadow mask, followed by spin coating of the polydimethylsiloxane (PDMS) with the thickness of 5 μm as an adhesive layer to the PVA sheet. The IG precursor was poured into the hole of the polyimide shadow mask. The doctor-blade coating was used to remove the excess amount of precursor from the holes. After solidification of the precursor, the shadow mask was removed. The upper electrode was transferred to form the metal-IG-metal configuration.

Device characterization: The electrical measurement was carried out with the electrochemical impedance analyzer (HIOKI, IM3590) in a glovebox filled with 1-atm nitrogen. The temperature sensor was placed on the heater to investigate the change of the capacitance and the ionic conductance at various temperatures from 30˚C to 80˚C, where temperature was calibrated with a temperature sensor (SATOTECH, CENTER376). The response time measurements were conducted by placing a glass plate warmed to 40˚C on the temperature sensor. Signals for multipoint sensing was retrieved by homemade electrical switching system.

ASSOCIATED CONTENT

Supporting Information.

Additional information related to surface profile of PVA film; samples for tensile-strain test

AUTHOR INFORMATION

Corresponding Author

Shunsuke Yamada Research Organization for Nano & Life Innovation, Waseda University, 3-4-1 Ookubo, Shinjuku, Tokyo 169-8555, Japan

orcid.org/0000-0002-9084-2070;

e-mail: santa.tokyo.ac.jp@gmail.com

ACKNOWLEDGMENT

This work was supported in part by JST CREST Grant No. JPMJCR15Q4, Japan, JSPS Grant-in-Aid for Research Activity start-up 19K23523, Japan, and the grant funding from the Tateisi Science and Technology Foundation 2187012.

REFERENCES

(1) Tee, B. C.-K.; Chortos, A.; Berndt, A.; Nguyen, A. K.; Tom, A.; McGuire, A.; Lin, Z. C.; Tien, K.; Bae, W.-G.; Wang, H.; Mei, P.; Chou, H.-H.; Cui, B.; Deisseroth, K.; Ng, T. N.; Bao, Z. A Skin-Inspired Organic Digital Mechanoreceptor. *Science (80-.)*. **2015**, *350* (6258), 313 LP – 316.

(2) Chou, H.-H.; Nguyen, A.; Chortos, A.; To, J. W. F.; Lu, C.; Mei, J.; Kurosawa, T.; Bae, W.-G.; Tok, J. B.-H.; Bao, Z. A Chameleon-Inspired Stretchable Electronic Skin with Interactive Colour Changing Controlled by Tactile Sensing. *Nat. Commun.* **2015**, *6*, 8011. https://doi.org/10.1038/ncomms9011.

(3) Kaltenbrunner, M.; Sekitani, T.; Reeder, J.; Yokota, T.; Kuribara, K.; Tokuhara, T.; Drack, M.; Schwödiauer, R.; Graz, I.; Bauer-Gogonea, S.; Bauer, S.; Someya, T. An

Ultra-Lightweight Design for Imperceptible Plastic Electronics. *Nature* **2013**, *499* (7459), 458–463. https://doi.org/10.1038/nature12314.

(4) Chen, L. Y.; Tee, B. C.-K.; Chortos, A. L.; Schwartz, G.; Tse, V.; J Lipomi, D.; Wong, H.-S. P.; McConnell, M. V; Bao, Z. Continuous Wireless Pressure Monitoring and Mapping with Ultra-Small Passive Sensors for Health Monitoring and Critical Care. *Nat. Commun.* **2014**, *5*, 5028. https://doi.org/10.1038/ncomms6028.

(5) Wang, S.; Xu, J.; Wang, W.; Wang, G.-J. N.; Rastak, R.; Molina-Lopez, F.; Chung, J. W.; Niu, S.; Feig, V. R.; Lopez, J.; Lei, T.; Kwon, S.-K.; Kim, Y.; Foudeh, A. M.; Ehrlich, A.; Gasperini, A.; Yun, Y.; Murmann, B.; Tok, J. B.-H.; Bao, Z. Skin Electronics from Scalable Fabrication of an Intrinsically Stretchable Transistor Array. *Nature* **2018**, *555*, 83.

(6) Yan, C.; Wang, J.; Lee, P. S. Stretchable Graphene Thermistor with Tunable Thermal Index. *ACS Nano* **2015**, *9* (2), 2130–2137. https://doi.org/10.1021/nn507441c.

(7) Zhu, C.; Chortos, A.; Wang, Y.; Pfattner, R.; Lei, T.; Hinckley, A. C.; Pochorovski, I.; Yan, X.; To, J. W.-F.; Oh, J. Y.; Tok, J. B.-H.; Bao, Z.; Murmann, B. Stretchable Temperature-Sensing Circuits with Strain Suppression Based on Carbon Nanotube Transistors. *Nat. Electron.* **2018**, *1* (3), 183–190. https://doi.org/10.1038/s41928-018-0041-0.

(8) Li, Y.; Ma, Y.; Wei, C.; Luan, H.; Xu, S.; Han, M.; Zhao, H.; Liang, C.; Yang, Q.; Yang, Y.; Crawford, K. E.; Feng, X.; Huang, Y.; Rogers, J. A. Thin, Millimeter Scale Fingernail Sensors for Thermal Characterization of Nail Bed Tissue. *Adv. Funct. Mater.* **2018**, *28* (30), 1801380. https://doi.org/10.1002/adfm.201801380.

(9) Yokota, T.; Inoue, Y.; Terakawa, Y.; Reeder, J.; Kaltenbrunner, M.; Ware, T.; Yang, K.; Mabuchi, K.; Murakawa, T.; Sekino, M.; Voit, W.; Sekitani, T.; Someya, T. Ultraflexible, Large-Area, Physiological Temperature Sensors for Multipoint Measurements. *Proc. Natl. Acad. Sci.* **2015**, *112* (47), 14533 LP – 14538. https://doi.org/10.1073/pnas.1515650112.

(10) Webb, R. C.; Bonifas, A. P.; Behnaz, A.; Zhang, Y.; Yu, K. J.; Cheng, H.; Shi, M.; Bian, Z.; Liu, Z.; Kim, Y.-S.; Yeo, W.-H.; Park, J. S.; Song, J.; Li, Y.; Huang, Y.; Gorbach, A. M.; Rogers, J. A. Ultrathin Conformal Devices for Precise and Continuous Thermal Characterization of Human Skin. *Nat. Mater.* **2013**, *12*, 938.

(11) Kim, Y.; Chortos, A.; Xu, W.; Liu, Y.; Oh, J. Y.; Son, D.; Kang, J.; Foudeh, A. M.; Zhu, C.; Lee, Y.; Niu, S.; Liu, J.; Pfattner, R.; Bao, Z.; Lee, T.-W. A Bioinspired Flexible Organic Artificial Afferent Nerve. *Science (80-.).* **2018**, *360* (6392), 998 LP – 1003. https://doi.org/10.1126/science.aao0098.

(12) Shen, J.-X.; Shang, D.-S.; Chai, Y.-S.; Wang, S.-G.; Shen, B.-G.; Sun, Y. Mimicking Synaptic Plasticity and Neural Network Using Memtranstors. *Adv. Mater.* **2018**, *30* (12), 1706717. https://doi.org/10.1002/adma.201706717.

(13) Kim, S.; Choi, B.; Lim, M.; Yoon, J.; Lee, J.; Kim, H.-D.; Choi, S.-J. Pattern Recognition Using Carbon Nanotube Synaptic Transistors with an Adjustable Weight Update Protocol. *ACS Nano* **2017**, *11* (3), 2814–2822. https://doi.org/10.1021/acsnano.6b07894.

(14) Salvatore, G. A.; Sülzle, J.; Dalla Valle, F.; Cantarella, G.; Robotti, F.; Jokic, P.; Knobelspies, S.; Daus, A.; Büthe, L.; Petti, L.; Kirchgessner, N.; Hopf, R.; Magno, M.; Tröster, G. Biodegradable and Highly Deformable Temperature Sensors for the Internet of

Things. *Adv. Funct. Mater.* **2017**, *27* (35), 1702390. https://doi.org/10.1002/adfm.201702390.

(15) Hwang, S.-W.; Tao, H.; Kim, D.-H.; Cheng, H.; Song, J.-K.; Rill, E.; Brenckle, M. A.; Panilaitis, B.; Won, S. M.; Kim, Y.-S.; Song, Y. M.; Yu, K. J.; Ameen, A.; Li, R.; Su, Y.; Yang, M.; Kaplan, D. L.; Zakin, M. R.; Slepian, M. J.; Huang, Y.; Omenetto, F. G.; Rogers, J. A. A Physically Transient Form of Silicon Electronics. *Science (80-.).* **2012**, *337* (6102), 1640 LP – 1644.

(16) Kang, S.; Murphy, R. K. J.; Hwang, S.; Lee, S. M.; Daniel, V.; Shin, J.; Gamble, P.; Cheng, H.; Yu, S.; Liu, Z.; Mccall, J. G.; Stephen, M.; Ying, H.; Kim, J.; Park, G.; Webb, R. C.; Lee, C. H.; Chung, S.; Wie, D. S.; Gujar, A. D.; Vemulapalli, B.; Kim, A. H.; Lee, K.; Cheng, J.; Huang, Y.; Lee, S. H.; Paul, V. Bioresorbable Silicon Electronic Sensors for the Brain. *Nature* **2016**. https://doi.org/10.1038/nature16492.

(17) Boutry, C. M.; Nguyen, A.; Lawal, Q. O.; Chortos, A.; Rondeau-Gagné, S.; Bao, Z. A Sensitive and Biodegradable Pressure Sensor Array for Cardiovascular Monitoring. *Adv. Mater.* **2015**, *27* (43), 6954–6961. https://doi.org/10.1002/adma.201502535.

(18) Curry, E. J.; Ke, K.; Chorsi, M. T.; Wrobel, K. S.; Miller, A. N.; Patel, A.; Kim, I.; Feng, J.; Yue, L.; Wu, Q.; Kuo, C.-L.; Lo, K. W.-H.; Laurencin, C. T.; Ilies, H.; Purohit, P. K.; Nguyen, T. D. Biodegradable Piezoelectric Force Sensor. *Proc. Natl. Acad. Sci.* **2018**, *115* (5), 909 LP – 914. https://doi.org/10.1073/pnas.1710874115.

(19) Gao, W.; Emaminejad, S.; Nyein, H. Y. Y.; Challa, S.; Chen, K.; Peck, A.; Fahad, H. M.; Ota, H.; Shiraki, H.; Kiriya, D.; Lien, D.-H.; Brooks, G. A.; Davis, R. W.; Javey, A. Fully

Integrated Wearable Sensor Arrays for Multiplexed in Situ Perspiration Analysis. *Nature* **2016**, *529*, 509.

(20) Sun, J.-Y.; Keplinger, C.; Whitesides, G. M.; Suo, Z. Ionic Skin. *Adv. Mater.* **2014**, *26* (45), 7608–7614. https://doi.org/10.1002/adma.201403441.

(21) Armand, M.; Endres, F.; MacFarlane, D. R.; Ohno, H.; Scrosati, B. Ionic-Liquid Materials for the Electrochemical Challenges of the Future. *Nat. Mater.* **2009**, *8* (8), 621–629. https://doi.org/10.1038/nmat2448.

(22) Earle, M. J.; Esperança, J. M. S. S.; Gilea, M. A.; Canongia Lopes, J. N.; Rebelo, L. P. N.; Magee, J. W.; Seddon, K. R.; Widegren, J. A. The Distillation and Volatility of Ionic Liquids. *Nature* **2006**, *439*, 831.

(23) Goossens, K.; Lava, K.; Bielawski, C. W.; Binnemans, K. Ionic Liquid Crystals: Versatile Materials. *Chem. Rev.* **2016**, *116* (8), 4643–4807. https://doi.org/10.1021/cr400334b.

(24) Osada, I.; de Vries, H.; Scrosati, B.; Passerini, S. Ionic-Liquid-Based Polymer Electrolytes for Battery Applications. *Angew. Chemie Int. Ed.* **2016**, *55* (2), 500–513. https://doi.org/10.1002/anie.201504971.

(25) Ma, Z.; Yu, J.; Dai, S. Preparation of Inorganic Materials Using Ionic Liquids. *Adv. Mater.* **2010**, *22* (2), 261–285. https://doi.org/10.1002/adma.200900603.

(26) Shunsuke, Y.; Hiroshi, T. A Water Dissolvable Electrolyte with an Ionic Liquid for Eco-Friendly Electronics. *Small* **2018**, *0* (0), 1800937. https://doi.org/10.1002/smll.201800937.

(27) Zhang, Y.; Yan, R.; Zhao, F.; Zeng, B. Polyvinyl Alcohol–Ionic Liquid Composition for Promoting the Direct Electron Transfer and Electrocatalysis of Hemoglobin. *Colloids Surfaces B Biointerfaces* **2009**, *71* (2), 288–292. https://doi.org/https://doi.org/10.1016/j.colsurfb.2009.03.001.

(28) Balo, L.; Shalu; Gupta, H.; Kumar Singh, V.; Kumar Singh, R. Flexible Gel Polymer Electrolyte Based on Ionic Liquid EMIMTFSI for Rechargeable Battery Application. *Electrochim. Acta* **2017**, *230*, 123–131. https://doi.org/https://doi.org/10.1016/j.electacta.2017.01.177.

(29) Lewandowski, A.; Świderska, A. New Composite Solid Electrolytes Based on a Polymer and Ionic Liquids. *Solid State Ionics* **2004**, *169* (1), 21–24. https://doi.org/https://doi.org/10.1016/j.ssi.2003.02.004.

(30) Yue, L.; Ma, J.; Zhang, J.; Zhao, J.; Dong, S.; Liu, Z.; Cui, G.; Chen, L. All Solid-State Polymer Electrolytes for High-Performance Lithium Ion Batteries. *Energy Storage Mater.* **2016**, *5*, 139–164. https://doi.org/https://doi.org/10.1016/j.ensm.2016.07.003.

(31) Sánchez, L. G.; Espel, J. R.; Onink, F.; Meindersma, G. W.; Haan, A. B. de. Density, Viscosity, and Surface Tension of Synthesis Grade Imidazolium, Pyridinium, and Pyrrolidinium Based Room Temperature Ionic Liquids. *J. Chem. Eng. Data* **2009**, *54* (10), 2803–2812. https://doi.org/10.1021/je800710p.

(32) Okoturo, O. O.; VanderNoot, T. J. Temperature Dependence of Viscosity for Room Temperature Ionic Liquids. *J. Electroanal. Chem.* **2004**, *568*, 167–181. https://doi.org/https://doi.org/10.1016/j.jelechem.2003.12.050.

(33) Ghatee, M. H.; Zare, M.; Moosavi, F.; Zolghadr, A. R. Temperature-Dependent Density and Viscosity of the Ionic Liquids 1-Alkyl-3-Methylimidazolium Iodides: Experiment and Molecular Dynamics Simulation. *J. Chem. Eng. Data* **2010**, *55* (9), 3084–3088. https://doi.org/10.1021/je901092b.

(34) Ota, H.; Chen, K.; Lin, Y.; Kiriya, D.; Shiraki, H.; Yu, Z.; Ha, T.-J.; Javey, A. Highly Deformable Liquid-State Heterojunction Sensors. *Nat. Commun.* **2014**, *5*, 5032. https://doi.org/10.1038/ncomms6032.

(35) Gui, Q.; He, Y.; Gao, N.; Tao, X.; Wang, Y. A Skin-Inspired Integrated Sensor for Synchronous Monitoring of Multiparameter Signals. *Adv. Funct. Mater.* **2017**, *27* (36), 1702050. https://doi.org/10.1002/adfm.201702050.

(36) Aldrich Chemical Co., I. Ionic Liquid. *ChemFiles* **2006**, *6* (9), 1–20.

(37) Watanabe, Y.; Morita, M.; Hamada, N.; Tsujisaka, Y. Formation of Hydrogen Peroxide by a Polyvinyl Alcohol Degrading Enzyme. *Agric. Biol. Chem.* **1975**, *39* (12), 2447–2448. https://doi.org/10.1080/00021369.1975.10861980.

(38) Sakai, K.; Hamada, N.; Watanabe, Y. Degradation Mechanism of Poly(Vinyl Alcohol) by Successive Reactions of Secondary Alcohol Oxidase and β-Diketone Hydrolase from Pseudomonas Sp. *Agric. Biol. Chem.* **1986**, *50* (4), 989–996. https://doi.org/10.1080/00021369.1986.10867494.

(39) Watanabe, Y.; Hamada, N.; Morita, M.; Tsujisaka, Y. Purification and Properties of a Polyvinyl Alcohol-Degrading Enzyme Produced by a Strain of Pseudomonas. *Arch.*

Biochem. Biophys. **1976**, *174* (2), 575–581. https://doi.org/https://doi.org/10.1016/0003-9861(76)90386-6.

(40) Ding, D.; Guerette, P. A.; Fu, J.; Zhang, L.; Irvine, S. A.; Miserez, A. From Soft Self-Healing Gels to Stiff Films in Suckerin-Based Materials Through Modulation of Crosslink Density and β-Sheet Content. *Adv. Mater.* **2015**, *27* (26), 3953–3961. https://doi.org/10.1002/adma.201500280.

(41) Butcher, D. T.; Alliston, T.; Weaver, V. M. A Tense Situation: Forcing Tumour Progression. *Nat. Rev. Cancer* **2009**, *9*, 108.

(42) Hu, X.; Cebe, P.; Weiss, A. S.; Omenetto, F.; Kaplan, D. L. Protein-Based Composite Materials. *Mater. Today* **2012**, *15* (5), 208–215. https://doi.org/https://doi.org/10.1016/S1369-7021(12)70091-3.

(43) Agache, P. G.; Monneur, C.; Leveque, J. L.; De Rigal, J. Mechanical Properties and Young's Modulus of Human Skin in Vivo. *Arch. Dermatol. Res.* **1980**, *269* (3), 221–232. https://doi.org/10.1007/BF00406415.

(44) Bergel, D. H. The Static Elastic Properties of the Arterial Wall. *J. Physiol.* **1961**, *156* (3), 445—457. https://doi.org/10.1113/jphysiol.1961.sp006686.

(45) Feng, Y. N.; Li, Y. P.; Liu, C. L.; Zhang, Z. J. Assessing the Elastic Properties of Skeletal Muscle and Tendon Using Shearwave Ultrasound Elastography and MyotonPRO. *Sci. Rep.* **2018**, *8* (1), 17064. https://doi.org/10.1038/s41598-018-34719-7.

(46) Dagdeviren, C.; Su, Y.; Joe, P.; Yona, R.; Liu, Y.; Kim, Y.-S.; Huang, Y.; Damadoran, A. R.; Xia, J.; Martin, L. W.; Huang, Y.; Rogers, J. A. Conformable Amplified Lead

Zirconate Titanate Sensors with Enhanced Piezoelectric Response for Cutaneous Pressure Monitoring. *Nat. Commun.* **2014**, *5* (1), 4496. https://doi.org/10.1038/ncomms5496.

(47) Choi, W. M.; Song, J.; Khang, D.-Y.; Jiang, H.; Huang, Y. Y.; Rogers, J. A. Biaxially Stretchable "Wavy" Silicon Nanomembranes. *Nano Lett.* **2007**, *7* (6), 1655–1663. https://doi.org/10.1021/nl0706244.

(48) Lee, W.; Kim, D.; Matsuhisa, N.; Nagase, M.; Sekino, M.; Malliaras, G. G.; Yokota, T.; Someya, T. Transparent, Conformable, Active Multielectrode Array Using Organic Electrochemical Transistors. *Proc. Natl. Acad. Sci.* **2017**, 201703886. https://doi.org/10.1073/pnas.1703886114.

(49) Keplinger, C.; Sun, J.-Y.; Foo, C. C.; Rothemund, P.; Whitesides, G. M.; Suo, Z. Stretchable, Transparent, Ionic Conductors. *Science (80-.).* **2013**, *341* (6149), 984–987. https://doi.org/10.1126/science.1240228.

(50) Yuguchi, Y.; Fujiwara, T.; Miwa, H.; Shirakawa, M.; Yajima, H. Color Formation and Gelation of Xyloglucan Upon Addition of Iodine Solutions. *Macromol. Rapid Commun.* **2005**, *26* (16), 1315–1319. https://doi.org/10.1002/marc.200500283.

(51) Wu, J.; Han, S.; Yang, T.; Li, Z.; Wu, Z.; Gui, X.; Tao, K.; Miao, J.; Norford, L. K.; Liu, C.; Huo, F. Highly Stretchable and Transparent Thermistor Based on Self-Healing Double Network Hydrogel. *ACS Appl. Mater. Interfaces* **2018**, *10* (22), 19097–19105. https://doi.org/10.1021/acsami.8b03524.

(52) Tokuda, H.; Tsuzuki, S.; Susan, M. A. B. H.; Hayamizu, K.; Watanabe, M. How Ionic Are Room-Temperature Ionic Liquids? An Indicator of the Physicochemical Properties. *J. Phys. Chem. B* **2006**, *110* (39), 19593–19600. https://doi.org/10.1021/jp064159v.

(53) Bhargava, B. L.; Balasubramanian, S. Layering at an Ionic Liquid–Vapor Interface: A Molecular Dynamics Simulation Study of [Bmim][PF6]. *J. Am. Chem. Soc.* **2006**, *128* (31), 10073–10078. https://doi.org/10.1021/ja060035k.

(54) Silva, F.; Gomes, C.; Figueiredo, M.; Costa, R.; Martins, A.; Pereira, C. M. The Electrical Double Layer at the [BMIM][PF6] Ionic Liquid/Electrode Interface – Effect of Temperature on the Differential Capacitance. *J. Electroanal. Chem.* **2008**, *622* (2), 153–160. https://doi.org/https://doi.org/10.1016/j.jelechem.2008.05.014.

(55) Ye, Y.-S.; Rick, J.; Hwang, B.-J. Ionic Liquid Polymer Electrolytes. *J. Mater. Chem. A* **2013**, *1* (8), 2719–2743. https://doi.org/10.1039/C2TA00126H.

(56) Sim, K.; Rao, Z.; Zou, Z.; Ershad, F.; Lei, J.; Thukral, A.; Chen, J.; Huang, Q.-A.; Xiao, J.; Yu, C. Metal Oxide Semiconductor Nanomembrane–Based Soft Unnoticeable Multifunctional Electronics for Wearable Human-Machine Interfaces. *Sci. Adv.* **2019**, *5* (8), eaav9653. https://doi.org/10.1126/sciadv.aav9653.

(57) Wang, Y.; Zhu, C.; Pfattner, R.; Yan, H.; Jin, L.; Chen, S.; Molina-Lopez, F.; Lissel, F.; Liu, J.; Rabiah, N. I.; Chen, Z.; Chung, J. W.; Linder, C.; Toney, M. F.; Murmann, B.; Bao, Z. A Highly Stretchable, Transparent, and Conductive Polymer. *Sci. Adv.* **2017**, *3* (3), e1602076. https://doi.org/10.1126/sciadv.1602076.

(58) Jimbo, Y.; Matsuhisa, N.; Lee, W.; Zalar, P.; Jinno, H.; Yokota, T.; Sekino, M.; Someya, T. Ultraflexible Transparent Oxide/Metal/Oxide Stack Electrode with Low Sheet Resistance for Electrophysiological Measurements. *ACS Appl. Mater. Interfaces* **2017**, *9* (40), 34744–34750. https://doi.org/10.1021/acsami.7b12802.

(59) Lee, G.; Kang, S.; Won, S. M.; Gutruf, P.; Jeong, Y. R.; Koo, J.; Lee, S.; Rogers, J. A.; Ha, J. S. Fully Biodegradable Microsupercapacitor for Power Storage in Transient Electronics. **2017**, *1700157*, 1–12. https://doi.org/10.1002/aenm.201700157.

Table of Contents Graphic